Measurement and interpretation of active Balmer alpha spectra at ASDEX Upgrade

B. Geiger[1], R. Dux[1], M. Dunne [1], A. Lebschy[1], R. McDermott[1], R. Reimer[2], M. Salewski[3], G. Tardini[1], M. Weiland[1] and the ASDEX Upgrade team[1]

[1]*Max-Planck-Institute for Plasma Physics, Garching, Germany,* [2]*Max-Planck-Institute for Plasma Physics, Greifswald, Germany,* [3]*Technical University of Denmark, Lyngby, Denmark*

Introduction

Active Balmer alpha spectroscopy has become an important diagnostic technique in fusion devices because it allows investigation of the main-ion temperature and rotation [1], the fast-ion density [2] and the magnetic field structure [3]. The technique is based on the observation of Balmer alpha radiation (656.1 nm, n=3->2), emitted by deuterium neutrals that are present along neutral beam injection (NBI) lines. Besides the injected neutrals, also main ions and fast ions can be analyzed because these get neutralized by charge exchange reactions and subsequently emit light. An example spectrum is plotted in figure 1, which shows the active components of Balmer alpha spectra (passive radiation, measured when neutral beam injection was turned off, has been subtracted). In addition to the measurement, simulated contributions are illustrated (from FIDASIM).

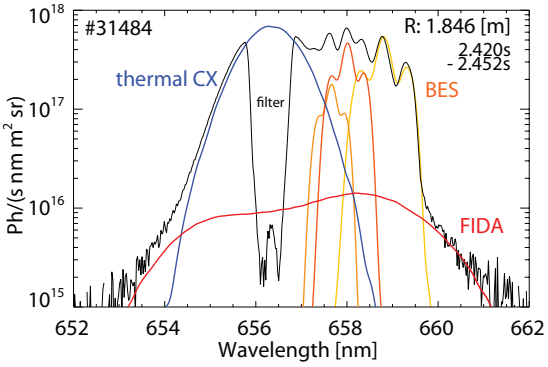

Figure 1: *Measured and simulated active Balmer alpha spectrum.*

The predicted beam emission (BES) is plotted in shades of orange. It is emitted by the injected neutrals after excitation through collisions with electrons and ions and can be subdivided into three energy components with different Doppler shifts: positive neutral beams, as applied here, inject full, half and one third energy neutrals. The spectral shape of the individual energy components is dominated by the Stark effect since the injected neutrals experience a strong $\mathbf{v}_{NBI} \times \mathbf{B}$ Lorentz electric field. This splits the radiation into three major peaks. The distance between these peaks depends on the orientation and strength of the magnetic field and, hence, allows to obtain information on the magnetic equilibrium. In blue is illustrated the simulated main ion charge exchange radiation, which can be described very well by a Gaussian curve. By analyzing the spectral width and Doppler shift of this component, main ion temperatures and rotations can be determined. The predicted charge exchange radiation emitted by fast beam ions (also called fast-ion D-alpha (FIDA) radiation) is illustrated in red in figure 1. A TRANSP [5] predicted fast-ion distribution function has been input to FIDASIM to consistently model the radiation. As can be seen, the FIDA component has broad wings and an asymmetric shape which contains information on fast-ion densities and the fast-ion velocity space distribution.

Diagnostic setup

In the ASDEX Upgrade tokamak, a new Balmer alpha diagnostic has been installed that can address all topics mentioned above. The diagnostic has been built in the framework of a major charge exchange recombination spectroscopy (CXRS) diagnostic installation that makes use of an array of 70 lines of sight (LOS). Figure 2 shows a sketch of these LOS, which intersect the 93 keV heating beam, labeled NBI Q8, at various positions from the low-field-side to the high-field-side.

21 of the LOS are foreseen for beam emission spectroscopy (BES) measurements while the others are used for the CXRS analysis of impurity ions. The BES spectrometer setup is shown in the lower right of figure 2. It is based on the Czerny turner approach with a 2000 lines/mm reflection grating and uses two 200 mm, F/2.0 lenses instead of mirrors. 22 fibers with $400\mu m$ diameter can be connected at its entrance and the application of two more lenses (56 mm, F/1.4 and 42 mm, F/0.95) allows us to block passive radiation at 656.1 nm, which would lead to saturation of the attached CCD camera. The additional lenses focus an intermediate image, of which parts are blocked by a wire, slightly de-magnified on the CCD camera. The effect of the wire can be seen in figure 1 since the measured spectrum is close to zero between 655 nm and 657 nm. The spectral range covered by this spectrometer approach is 15 nm and the spectral resolution is 0.05 nm. The latter is determined mainly by the entrance slit, which is set to a width of 50 μm.

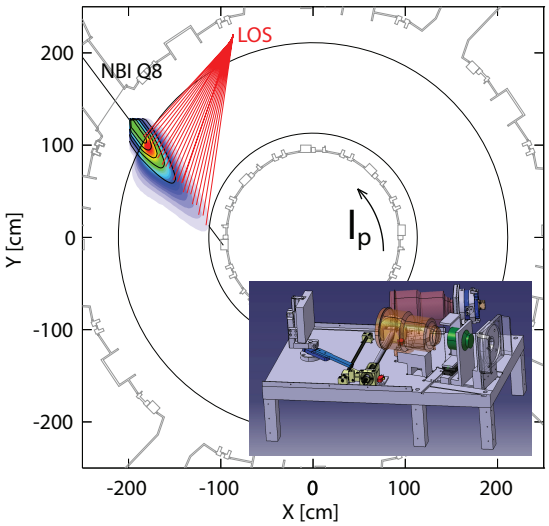

Figure 2: *Top-down view showing the LOS setup in red and a contour plot of the neutral density during operation of NBI Q8.*

Study of the magnetic field structure

The good spectral resolution of the diagnostic allows us to investigate the beam emission very accurately. Figure 3 shows a contour plot of the beam emission measured in discharge #31484 (B_t=-2.5 T, I_p=800 kA). Clearly, the beam emission is attenuated towards smaller radii R where it exhibits larger Doppler shifts and a stronger Stark splitting. The larger Doppler shifts are explained by the viewing geometry of the diagnostic. The angles between LOS and NBI Q8 become less perpendicular at lower radii, i.e. change from 83 degree to 77 degree. The strong splitting at low radii is well explained by the 1/R dependence of the toroidal field and allows us to clearly identify the independent Stark lines. In contrast

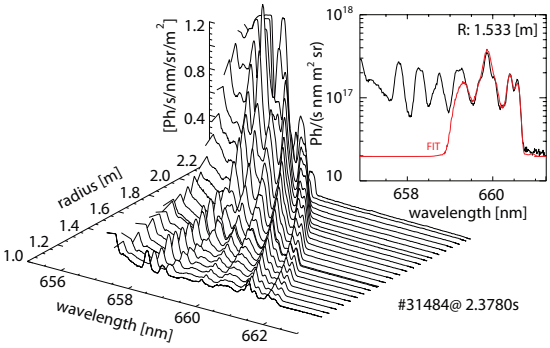

Figure 3: *Measured beam emission as a function of radius and wavelength.*

to the observed 3 major peaks per energy-component on the low-field side (see figure 1), the beam emission observed at the high-field-side allows us to study the Stark spectrum with its 9 transitions [6] (see upper right plot of figure 3). By fitting the spectra with an accurate model including the detailed shape of each Stark line [6], the distance of the individual lines and, therefore, the strength of the $\mathbf{v}_{NBI} \times \mathbf{B}$ electric field can be determined.

Figure 4 compares a measured radial $\mathbf{v}_{NBI} \times \mathbf{B}$ profile with profiles resulting from different equilibrium reconstructions (the corresponding q-profiles are displayed in the sub-plot). The error-bars of the measurement represent the statistical noise withing 5 subsequent time points, measured with 5 ms exposure time. Clearly, the equilibrium with the very low q-profile plotted in blue does not represent the measurement. This already shows that the BES measurement may allow us to improve future equilibrium reconstructions within a Bayesian framework.

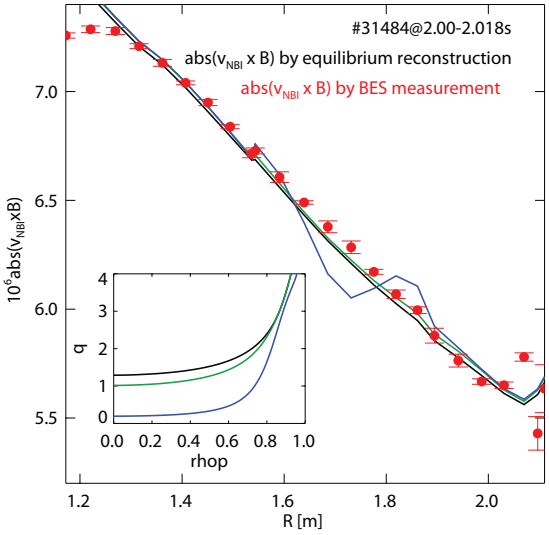

Figure 4: *Measured $\mathbf{v}_{NBI} \times \mathbf{B}$ profile compared with equilibrium reconstructions.*

Main ion T_i and v_{tor}

The main ion temperature, T_i, and rotation, v_{tor}, can be determined by fitting the thermal charge exchange component with a Gaussian curve. This is well within the abilities of our diagnostic setup because the beam emission is, in particular on the high-field-side, shifted far away.

In figure 5, we show radial profiles of the measured main-ion temperature and main-ion rotation with error-bars that represent the statistical noise. No data is shown for R<1.35 m and R>1.95 m because there, too low active signals and too strong overlap with the beam-emission prevent the analysis, respectively. The measured profiles have been corrected by cross-section effects, velocity space effects and a reduced radial resolution using the FIDASIM code: Based on the measured apparent [1] temperature and rotation, we calculated synthetic main-ion spectra and fitted them with a Gaussian curve. The ratios between the profiles input to FIDASIM and the fitted apparent temperature and rotation profiles have been used to correct the measurement. In addition to the direct measurement, figure 5 illustrates in black the temperature and rotation of nitrogen from which main-ion profiles have been determined neoclassically using TRANSP (blue). In particular in the plasma center, the main-ion measurement exceeds the temperatures from the nitrogen measurement and better agreement is found with the measured electron temperature profile, plotted

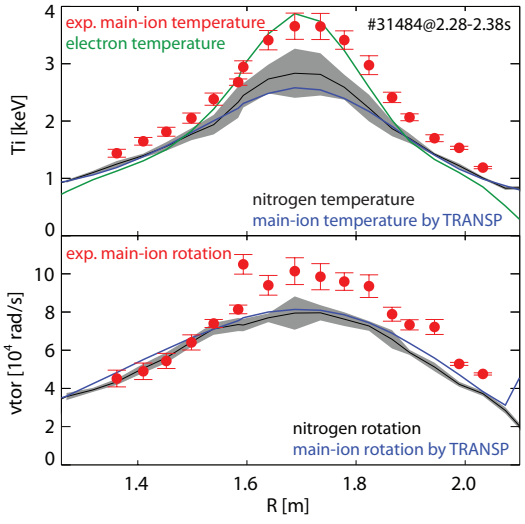

Figure 5: *Temperature and rotation profiles.*

in green. The directly measured main-ion rotations roughly agree within the error-bars with the ones determined using nitrogen but are systematically larger. The origin of this discrepancy is not yet clear and will be the subject to more detailed investigations.

Fast-ion D-alpha

The presence of the beam emission and the main-ion radiation in the spectra restricts the observable fast-ion radiation to large Doppler shifts. The velocity space observed at such wavelengths is displayed in color in figure 6 for a central LOS and for two wavelength ranges. In addition, the TRANSP predicted fast-ion velocity space distribution for discharge #30841 (similar to #31484) is displayed, which mainly exhibits positive pitch values ($v_{||}/v_{tot}$), well explained by the co-current NBI geometry. The overlap between the fast-ion distribution function and the weight function for wavelengths between 651 nm and 652 nm is very small. This explains the absence of FIDA radiation in figure 1 in this wavelength range. Better overlap with the weight function is observed for wavelengths between 661 nm and 662 nm, which is in agreement with the red-shifted FIDA contribution in figure 1. Radial profiles of the FIDA radiation, integrated between 661 nm and 662 nm and normalized by the measured level of the beam emission, are shown in figure 7. The comparison with the FIDASIM+TRANSP prediction shows good agreement, indicating that fast-ions are consistently modeled.

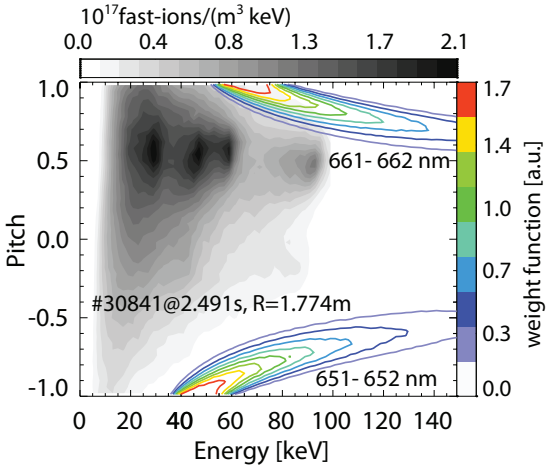

Figure 6: *Weight functions and fast-ion distribution function.*

Acknowledgement

This work has been carried out within the framework of the EUROfusion Consortium and has received funding from the Euratom research and training programme 2014-2018 under grant agreement No 633053. The views and opinions expressed herein do not necessarily reflect those of the European Commission.

References

[1] GRIERSON, B. A. et al., RSI **81** (2010)

[2] HEIDBRINK, W. W. et al., PPCF **46** (2004) 1855

[3] WOLF, R. et al., Nuclear Fusion **33** (1993) 1835

[4] HEIDBRINK, W. et al., Commun. Comput. Phys. **10** (2011) 716

[5] PANKIN, A. et al., Computer Physics Communications **159** (2004) 157

[6] DUX, R. et al., this proceeding **P1.121** (2015)

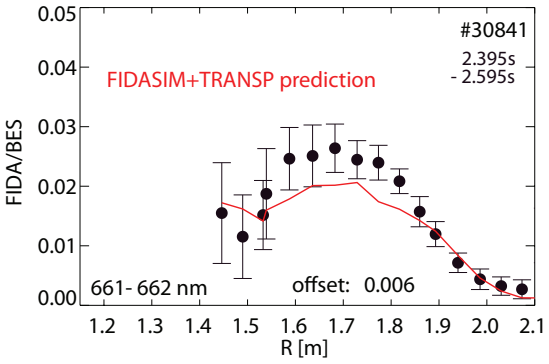

Figure 7: *Radial FIDA profile, normalized by the beam emission intensity and compared with the prediction from FIDASIM+TRANSP*